ACS APPLIED MATERIALS & INTERFACES

Research Article

Cite This: ACS Appl. Mater. Interfaces XXXX, XXX, XXX−XXX

www.acsami.org

Monitoring Local Electric Fields at Electrode Surfaces Using Surface Enhanced Raman Scattering-Based Stark-Shift Spectroscopy during Hydrogen Evolution Reactions

Haotian Shi,[†] Zhi Cai,[‡] Joel Patrow,[†] Bofan Zhao,[§] Yi Wang,[†] Yu Wang,[‡] Alexander Benderskii,[†] Jahan Dawlaty,[†] and Stephen B. Cronin*[,†,§]

[†]Department of Chemistry, [‡]Department of Materials Science, and [§]Ming Hsieh Department of Electrical Engineering, University of Southern California, Los Angeles, California 90089, United States

Supporting Information

ABSTRACT: We report the use of surface-enhanced Raman scattering (SERS) to measure the vibrational Stark shifts of surface-bound thiolated-benzonitrile molecules bound to an electrode surface during hydrogen evolution reactions (HERs). Here, the electrode surface consists of Au nanoislands deposited both with and without an underlying layer of monolayer graphene on a glass substrate. The Stark shifts observed in the nitrile (C−N) stretch frequency (around 2225 cm^{-1}) are used to report the local electric field strength at the electrode surface under electrochemical working conditions. Under positive (i.e., oxidative) applied potentials [vs normal hydrogen electrode (NHE)], we observe blue shifts of up to 7.6 cm^{-1}, which correspond to local electric fields of 22 mV/cm. Under negative applied potentials (vs NHE), the C−N stretch frequency is red-shifted by only about 1 cm^{-1}. This corresponds to a regime in which the electrochemical current increases exponentially in the hydrogen evolution process. Under these finite electrochemical currents, we estimate the voltage drop across the solution ($V = IR$). Correcting for this voltage drop results in a highly linear electric field versus applied electrochemical voltage relation. Here, the onset potential for the HER lies around 0.2 V versus NHE and the point of zero charge (PZC) occurs at 0.04 V versus NHE, based on the capacitance−voltage ($C-V$) profile. The solution field is obtained by comparing the C−N stretch frequency in solution with that obtained in air. By evaluating the local electric field strength at the PZC and the onset potential, we can separate the solution field from the reaction field (i.e., electrode field), respectively. At the onset of HER, the solution field is −0.8 mV/cm and the electrode field is −1.2 mV/cm. At higher ion concentrations, we observe similar electric field strengths and more linear E-field versus applied potential behavior because of the relatively low resistance of the solution, which results in negligible voltage drops ($V = IR$).

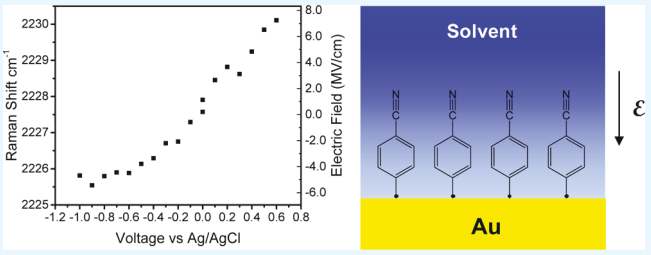

KEYWORDS: *vibrational fingerprint, sensing, detection, SERS, surface enhanced*

INTRODUCTION

Electrochemical reactions at solid/liquid interfaces represent complex processes, which include the application of an applied potential between the working and counter electrodes, binding of the reactant and intermediate species to the electrode surface, electrostatic fields within the double layer, diffusion of reactants in solution, and ultimately charge transfer to the ions in solution. There are loss mechanisms associated with each of these key components in the overall electrochemical efficiency. This complex process is often oversimplified to provide a basic interpretation of the experimental data, largely because simple methods for separating these key components do not yet exist. In the work presented here, we apply spectroscopic tools, that is, Stark-shift surface enhanced Raman scattering (SERS) spectroscopy, to study and separate the key components of the electrochemical process to improve our understanding of energy loss in this important energy conversion system. Large electrostatic fields exist at the surface of electrodes largely because of the electrochemical double layer at this solid/liquid interface.[1] Many chemical reactions involve charged or polarized reactants, transition states, and products. Electric fields can have a significant effect on any of these, and therefore, fields, reaction mechanisms, and catalysis are intimately related to the local electric field strength.

Using sum frequency generation (SFG) spectroscopy, Dawlaty and co-workers carried out a systematic study of the interfacial solvation effects on the nitrile frequency shift of mercaptobenzonitrile bound to gold electrode surfaces.[1,2] Although these prior Stark-shift spectroscopy measurements have elucidated the interfacial fields for the first time, there are several difficulties associated with SFG spectroscopy, the chief of which is the strong absorption of the infrared (IR) beam in

Received: July 17, 2018
Accepted: September 6, 2018
Published: September 6, 2018

DOI: 10.1021/acsami.8b11961
ACS Appl. Mater. Interfaces XXXX, XXX, XXX−XXX

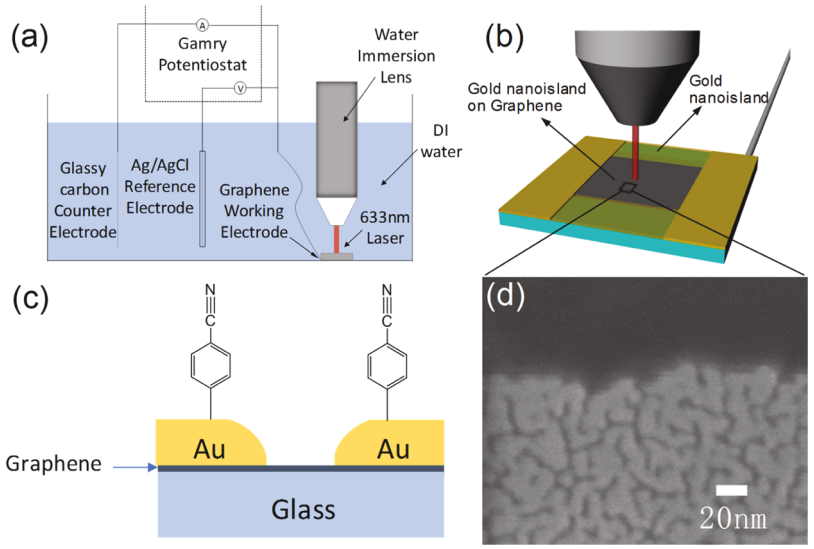

Figure 1. (a,b) Schematic diagrams of the three-terminal photoelectrochemical cell using a water immersion lens. (c) Cross-sectional diagram of the sample structure. (d) Scanning electron microscopy image of the 5 nm Au film.

water (electrolyte), which limits the optical path length to approximately 25 μm-thick microfluidic channels/cells. Also, substantial nonlinear optical mixing by other components of the system create a large background signal that can obscure the relatively small signal produced by the surface layer of molecules. As a result of these difficulties, there are only a handful of groups in the world that are capable of performing SFG measurements reliably. In the work presented here, we demonstrate the ability to perform Stark-shift spectroscopy using SERS, which is a far easier measurement to perform and has several additional advantages over SFG spectroscopy. In typical SFG measurements, the optical path length through the solution must be limited to 25 μm or less to minimize absorption of the IR beam, requiring elaborate microcell reactors to be employed. SERS eliminates the need for these microcell reactors, thus eliminating the large voltage drops associated with the series resistance of the electrolyte. SERS has much higher signals than SFG, enabling spectra to be acquired in seconds rather than in minutes, and higher signal-to-noise ratios.

SERS-based vibrational Stark shifts have been used previously to probe interfacial electric fields by Harris et al.[3,4] and Hildebrandt et al.[5] using roughened metal electrodes. In the work presented here, we deposit Au films nominally 5 nm in thickness by electron-beam evaporation in vacuum, which are not thick enough to form continuous films and instead create islandlike structures that are known to exhibit strong plasmon resonances, as shown in Figure 1d.[6−8] The Cronin group has studied these films extensively using the finite difference time domain method.[9,10] The electric field response of these films is dominated by the small gaps between the islands, which produce intense electric field "hot spots." In these localized hot spot regions, the electric field intensity is 1000 times larger than the incident electric field, resulting in strong electromagnetic SERS enhancement.[9,10] Natelson and his co-workers have large, reversible, bias-driven Stark shifts using phenyl-C_{61}-butyric acid methyl ester/C_{60}−gold system to study SERS in the presence of electrostatic fields.[11,12] The use of surface-bound thiolated molecules is a key component of this spectroscopic approach as well as the use of a water immersion lens to measure these SERS spectra in situ under electrochemical working conditions. Measurement of SERS spectra under applied electrochemical or electrostatic potentials is referred to as "E-SERS," and there are only a handful of papers on this topic, mostly reporting irreversible changes in the spectra, and the results have not been reproduced by other groups.[13−18] In these previous SERS studies, the Stark-shifted fields were not correlated with the electrochemical current and point of zero charge (PZC), nor were solution fields taken into account. We use Stark-shift SERS spectroscopy to establish the electrostatic contribution to the reaction fields that take place at electrode surfaces in an electrochemical process. These interfacial fields have been difficult to establish experimentally but play an important role in the electrochemical process through the initiation of charge transfer and in determining the overpotentials required to drive reactions. Every molecule in a medium polarizes its surrounding environment, and the induced polarization creates a field that is, in turn, felt by the molecule. This is known as the solvation field, and this has important consequences for charge transfer at interfaces. By elucidating the electrostatics at the electrode/electrolyte interface, we develop a better understanding of the solvation fields near the interface. The PZC corresponds to the electrochemical potential above which the electrode becomes positively charged and drives oxidation half-reactions and below which it becomes negative and drives reduction half-reactions.[19] The surrounding electrolyte acquires an equal and opposite charge (i.e., double layer and Debye layer) forming a capacitor. At the PZC, the electrode and the surrounding electrolyte become charge neutral, and the capacitance is a minimum. What is fundamentally interesting about this study is the fact that the electric field at the electrode surface does not go zero at the charge neutrality point, as would be the case in a solid-state junction (e.g., pn-junction). This is due to the complex nature of the water/electrode interface.

EXPERIMENT

The electrodes used in our work presented here utilize an underlying monolayer of graphene grown by chemical vapor deposition (CVD) to electronically connect the 5 nm Au nanoislands. Monolayer graphene was grown by CVD at 1000

DOI: 10.1021/acsami.8b11961
ACS Appl. Mater. Interfaces XXXX, XXX, XXX−XXX

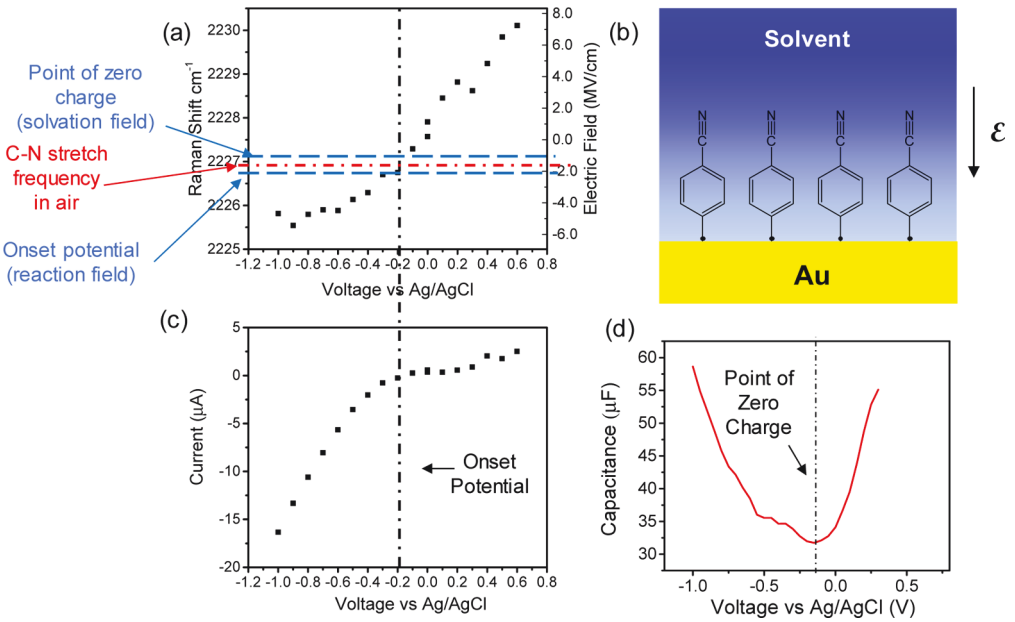

Figure 2. (a) Raman shift of the nitrile stretch and electric field strength plotted as a function of the applied electrochemical potential. (b) Schematic diagram illustrating the SERS measurement of thiolated-benzonitrile bound to an Au electrode for Stark-shift spectroscopy. (c) Current−voltage plotted as a function of the electrochemical potential, indicating the onset potential. (d) Electrochemical impedance spectroscopy obtained capacitance−voltage plot indicating the PZC.

°C in methane and H_2 gas on a copper foil at a reduced pressure of 1−1.5 Torr.[20] The copper foil with graphene was then coated with a thin layer of poly(methyl methacrylate) (PMMA)-A6 by spin-coating at 2000 rpm for 45 s and then baking at 150 °C for 5 min. Copper etchant was used to etch away the copper from the bottom of the "sandwich" structure, resulting in a graphene/PMMA film that is left floating on the surface of the liquid copper etchant. This film is then cleaned with 10% hydrochloric acid in deionized (DI) water.[21] Prior to transferring the graphene, two gold electrodes are deposited on a glass substrate by electron-beam evaporation using a shadow mask to serve as the target substrate. The PMMA/graphene layer was then scooped up on the target substrate connecting both gold electrodes. The sample was then baked at 120 °C for 5 min to improve adhesion. After this, the PMMA layer was removed with a 5 min acetone dip. A 5 nm (nominal thickness) Au film was then deposited on the sample using electron-beam evaporation. A thin layer of 4-mercaptobenzonitrile (4-MBN) molecules was deposited by soaking the sample in a 0.03 mol/L solution of 4-MBN in ethanol for 24 h,[2,22] resulting in the structure illustrated in Figure 1c. We attached copper wires to both gold electrodes and used this as our working electrode in a three-terminal potentiostat setup. The contact area between the copper wires and gold electrodes (coated with silver paint) were then encapsulated in epoxy so that they were not in contact with the electrolyte.

Raman spectra of 4-MBN were taken with 633 nm wavelength excitation (see Figure S1b of the Supporting Information), which is resonant with this molecule's absorption, under applied electrochemical potentials in pure DI water using a water immersion lens, as illustrated in Figure 1a. To protect the lens from the solution, it was covered with a 13 μm-thick Teflon sheet (American Durafilm, Inc.). A three-terminal potentiostat (Gamry, Inc.) was used to apply various electrochemical potentials to the graphene working electrode with respect to the reference electrode. A silver/silver chloride reference electrode and a glassy carbon electrode (SPI, Inc.) were used as the reference and counter electrodes, respectively. The monolayer graphene electrode (1 cm × 1 cm) typically has an in-plane resistance of 1−2 kΩ. Figure S1 in the Supporting Information shows the SERS spectra taken of thiolated benzonitrile on Au nanoislands deposited on a glass substrate both with and without the underlying graphene monolayer. We observe a strong Raman signal from the C−N nitrile stretch mode around 2225 cm^{-1} with a 20 s integration time and 0.1 mW laser power. It is also important to note that the rectification of plasmon resonance may also occur when using plasmonic structures to study Stark shifts.[23] Kwasnieski and co-workers reported that the CN stretch of MBN varies as function of optical power.[24] This implies that optical rectification of the plasmon-driven field can be used to change the surface potential. Nelson and Schultz has shown that this effect can even alter the surface reactivity.[25] However, according to Nelson's laser power-CN stretch relation, the laser power used in our work reported here (0.1 mW) is on the low end of powers inducing any appreciable surface optical rectification effects. At such low powers, the modulation optical rectification is expected to play a very limited role in the reaction on the surface.[25] Here, the conducting graphene layer reduces the SERS enhancement by a factor of approximately 5×. For Au nanoislands deposited on a continuous gold film (50 nm thick), however, the SERS effect is completely quenched, and there are no detectible Raman features of the MBN molecules on these structures. As such, the Au nanoisland system and the graphene/Au nanoisland system present a unique opportunity to study in situ SERS spectra at electrochemical interfaces.

RESULTS AND DISCUSSION

Figure 2a shows the Stark shifts of the C−N stretch mode of MBN bound to 5 nm Au nanoisland films (shown in Figure 1) using SERS. Figure 2a shows the voltage-induced shifts of the

DOI: 10.1021/acsami.8b11961
ACS Appl. Mater. Interfaces XXXX, XXX, XXX−XXX

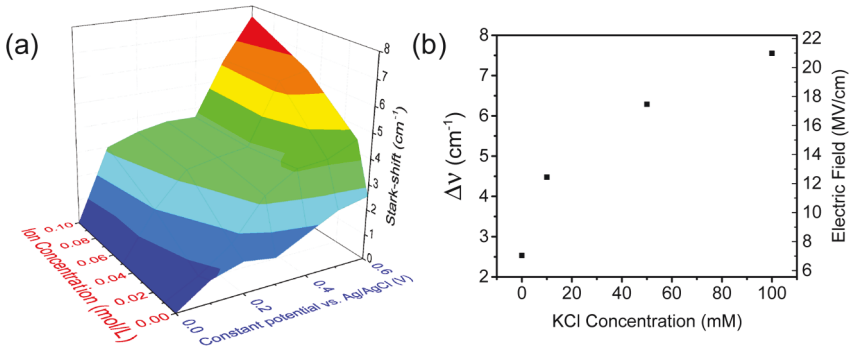

Figure 3. (a) Frequency change as a function of the applied potential and KCl ionic concentration. (b) Slice through this plot at a potential of 0.6 V vs Ag/AgCl reference electrode.

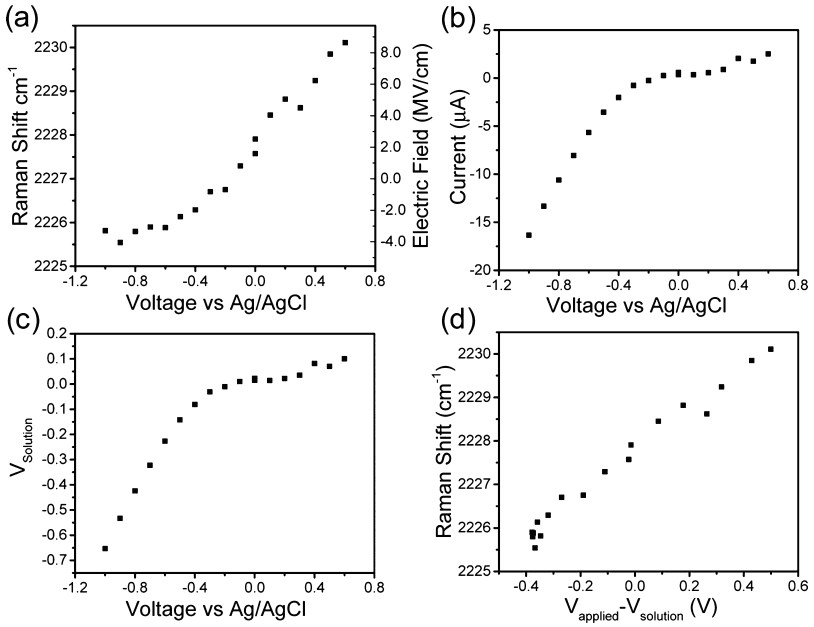

Figure 4. (a) Raman shift of the nitrile stretch and electric field strength plotted as a function of the applied electrochemical potential in 0.01 mol/L KCl solution. (b) Current−voltage plotted as a function of the electrochemical potential, indicating the onset potential. (c) Voltage drop across the solution calculated from (b). (d) Raman shift of the nitrile stretch plotted as a function of the corrected potential.

nitrile stretch mode (around 2225 cm^{-1}) plotted as a function of the applied electrochemical potential in pure water. These Stark shifts can be converted to electric field using $E = \Delta\omega_{C-N}/0.36$ [(mV/cm)/cm^{-1}] relation put forth by Boxer[26,27] and Dawlaty,[1,2] as indicated on the right axis of the plot. These Stark-shifted fields can be correlated with the onset potential and PZC obtained from the current−voltage ($I-V$) and capacitance−voltage ($C-V$) characteristics, as shown in Figure 2c,d, respectively. This is the first time these three datasets have been obtained simultaneously on the same electrode surface. Taken together, they enable us to separate the solvation (i.e., reaction) fields from the electrostatic fields produced by the electrode. Here, the onset potential for the hydrogen evolution reaction (HER) lies around 0 V versus normal hydrogen electrode (NHE) (−0.2 V vs Ag/AgCl) and the PZC occurs at 0.04 V versus NHE (−0.16 V vs Ag/AgCl), based on the capacitance−voltage profile. On the basis of the local electric field strength at the PZC ($E_{solution}$ = −0.8 mV/cm) and the onset potential (E_{onset} = −2.0 mV/cm), we can separate the solution field from the reaction field, respectively. Interestingly (or coincidentally), the solvation field −1.4 mV/cm (blue-shifted with respect to the C−N molecule in air) is quite close to the electrode field (−1.2 mV/cm) at the onset potential. Figure S3 in the Supporting Information is a waterfall plot showing the evolution of the entire Raman spectrum as a function of the applied potential. In addition to changes in the C−N mode position, the integrated intensity decreases and the line width increases with positively applied potentials, which is in good agreement with the results of Hildebrandt's work.[28] Other modes (other than C−N mode) also shift under the applied potentials. However, these shifts are substantially smaller than the C−N stretch mode, which is known to be particularly sensitive to externally applied electric fields.

We also studied the ionic strength dependence of these Stark shifts. Here, we repeated the voltage-dependent C−N stretch Stark-shift measurements in potassium chloride (KCl) solutions with different concentrations (0, 0.01, 0.05, and 0.1 mol/L). Figure 3 shows the electrochemical potential dependence of the Raman shifts and the corresponding electric fields

DOI: 10.1021/acsami.8b11961
ACS Appl. Mater. Interfaces XXXX, XXX, XXX−XXX

of the MBN molecule in various ionic strengths. In the three-dimensional plot (Figure 3a), we observe larger Stark shifts ($\Delta\nu$) in solutions with higher ionic strength. In pure water, the Stark shift is around 2.5 cm^{-1} when a potential of +0.6 V versus Ag/AgCl is applied. However, in 0.1 M KCl solution, we observe Stark shifts ($\Delta\nu$) up to 7.6 cm^{-1} at +0.6 V versus Ag/AgCl, which can be seen more clearly in Figure 3b, depicting a slice of the data shown in Figure 3a at an applied potential of +0.6 V versus Ag/AgCl. Empirically, we found that the MBN molecules were not stable at potentials above +0.6 V versus Ag/AgCl.

Figure 4a,b shows the original Stark shift versus voltage dependence and current−voltage ($I-V$) dependence obtained in 0.01 mol/L KCl solution. Here, a deviation from the linear relation between Raman shift and applied potential can be seen when the electrochemical current increases below approximately −0.3 V versus Ag/AgCl. This is due to the finite voltage drop across the solution (i.e., $V = IR$). Figure 4c shows an estimate of the voltage drop across the solution ($V_{solution}$) obtained by multiplying the electrochemical current in Figure 4b by the finite resistance of the electrolyte. Figure 4d plots the Raman shift as a function of the corrected voltage ($V_{applied} - V_{solution}$), which shows a more consistent linear dependence of the Raman Stark shift on the electrode potential.

CONCLUSIONS

We observe substantial shifts in the Raman spectra of surface-bound MBN molecules under various applied electrochemical potentials. The C−N stretch frequency is blue-shifted by as much as 7.6 cm^{-1} under an applied potential of 0.6 V (vs NHE), which corresponds to local electric fields of 22 mV/cm. Under −0.8 V applied potential (vs NHE), the C−N stretch frequency is red-shifted for only about 1 cm^{-1}, which is much less compared to the positive case. This corresponds to a regime in which the electrochemical current increases exponentially in the hydrogen evolution process. We believe that this saturation field corresponds to a substantial voltage drop across the solution ($V = IR$) under finite currents in the HER. On the basis of the $C-V$ measurement, the PZC occurs at 0.04 V versus NHE. The $I-V$ measurements shows that the onset potential for the HER lies around 0.2 V versus NHE. Comparing the C−N stretch frequency in solution with that obtained in air, we can calculate the solution field. Thus, the solution field is separated from the reaction field (i.e., electrode field) by assessing the local electric field strength at the onset potential and the PZC. At higher ion concentrations, similar electric field strengths and more E-field saturation at the onset potential are observed, which is due to the relatively low resistance of the solution ($V = IR$).

ASSOCIATED CONTENT

Supporting Information

The Supporting Information is available free of charge on the ACS Publications website at DOI: 10.1021/acsami.8b11961.

Schematic diagram of the in situ SERS measurements using a water immersion lens; SERS spectra taken of thiolated benzonitrile on Au nanoislands deposited on a glass substrate both with and without an underlying monolayer of graphene; cross-sectional diagram of the Au nanoislands/graphene on a glass sample structure; SERS spectra of thiolated benzonitrile on different regions of the sample; Au nanoislands deposited on a glass substrate both with and without an underlying monolayer of graphene with gold electrode; and waterfall plot of the raw Raman spectra under various applied potentials as indicated in the legend (PDF)

AUTHOR INFORMATION

Corresponding Author

*E-mail: scronin@usc.edu.

ORCID

Alexander Benderskii: 0000-0001-7031-2630
Jahan Dawlaty: 0000-0001-5218-847X
Stephen B. Cronin: 0000-0001-7089-6672

Notes

The authors declare no competing financial interest.

ACKNOWLEDGMENTS

This research was supported by NSF award no. 1708581 (H.S.), Army Research Office ARO award no. W911NF-14-1-0228 (Y.W.), NSF CAREER award no. 1454467 (J.P., J.D.), and Air Force Office of Scientific Research grant no. FA9550-15-1-0184 (B.Z.).

REFERENCES

(1) Sorenson, S. A.; Patrow, J. G.; Dawlaty, J. M. Solvation Reaction Field at the Interface Measured by Vibrational Sum Frequency Generation Spectroscopy. *J. Am. Chem. Soc.* **2017**, *139*, 2369−2378.

(2) Patrow, J. G.; Sorenson, S. A.; Dawlaty, J. M. Direct Spectroscopic Measurement of Interfacial Electric Fields near an Electrode under Polarizing or Current-Carrying Conditions. *J. Phys. Chem. C* **2017**, *121*, 11585−11592.

(3) Oklejas, V.; Sjostrom, C.; Harris, J. M. SERS Detection of the Vibrational Stark Effect from Nitrile-Terminated SAMs to Probe Electric Fields in the Diffuse Double-Layer. *J. Am. Chem. Soc.* **2002**, *124*, 2408−2409.

(4) Oklejas, V.; Sjostrom, C.; Harris, J. M. Surface-Enhanced Raman Scattering Based Vibrational Stark Effect as a Spatial Probe of Interfacial Electric Fields in the Diffuse Double Layer. *J. Phys. Chem. B* **2003**, *107*, 7788−7794.

(5) Schkolnik, G.; Salewski, J.; Millo, D.; Zebger, I.; Franzen, S.; Hildebrandt, P. Vibrational Stark Effect of the Electric-Field Reporter 4-Mercaptobenzonitrile as a Tool for Investigating Electrostatics at Electrode/SAM/Solution Interfaces. *Int. J. Mol. Sci.* **2012**, *13*, 7466.

(6) Kumar, R.; Zhou, H.; Cronin, S. B. Surface-enhanced Raman spectroscopy and correlated scanning electron microscopy of individual carbon nanotubes. *Appl. Phys. Lett.* **2007**, *91*, 223105.

(7) Kneipp, K.; Kneipp, H.; Corio, P.; Brown, S. D. M.; Shafer, K.; Motz, J.; Perelman, L. T.; Hanlon, E. B.; Marucci, A.; Dresselhaus, G.; Dresselhaus, M. S. Surface-enhanced and normal Stokes and anti-Stokes Raman spectroscopy of single-walled carbon nanotubes. *Phys. Rev. Lett.* **2000**, *84*, 3470−3473.

(8) Liu, Z.; Hou, W.; Pavaskar, P.; Aykol, M.; Cronin, S. B. Plasmon Resonant Enhancement of Photocatalytic Water Splitting Under Visible Illumination. *Nano Lett.* **2011**, *11*, 1111−1116.

(9) Pavaskar, P.; Theiss, J.; Cronin, S. B. Plasmonic hot spots: nanogap enhancement vs focusing effects from surrounding nanoparticles. *Opt. Express* **2012**, *20*, 14656−14662.

(10) Pavaskar, P.; Hsu, I. K.; Theiss, J.; Hung, W. H.; Cronin, S. B. A microscopic study of strongly plasmonic Au and Ag island thin films. *J. Appl. Phys.* **2013**, *113*, 034302.

(11) Li, Y.; Doak, P.; Kronik, L.; Neaton, J. B.; Natelson, D. Voltage tuning of vibrational mode energies in single-molecule junctions. *Proc. Natl. Acad. Sci. U.S.A.* **2014**, *111*, 1282−1287.

(12) Li, Y.; Zolotavin, P.; Doak, P.; Kronik, L.; Neaton, J. B.; Natelson, D. Interplay of Bias-Driven Charging and the Vibrational Stark Effect in Molecular Junctions. *Nano Lett.* **2016**, *16*, 1104−1109.

DOI: 10.1021/acsami.8b11961
ACS Appl. Mater. Interfaces XXXX, XXX, XXX−XXX

(13) Harroun, S. G.; Abraham, T. J.; Prudhoe, C.; Zhang, Y.; Scammells, P. J.; Brosseau, C. L.; Pye, C. C.; Singer, R. D. Electrochemical surface-enhanced Raman spectroscopy (E-SERS) of novel biodegradable ionic liquids. *Phys. Chem. Chem. Phys.* **2013**, *15*, 19205−19212.
(14) Kudelski, A.; Pettinger, B. Fluctuations of surface-enhanced Raman spectra of CO adsorbed on gold substrates. *Chem. Phys. Lett.* **2004**, *383*, 76−79.
(15) Sanchez, L. A.; Birke, R. L.; Lombardi, J. R. Surface-enhanced Raman scattering of piperidine. The effect of electrode potential on intensity. *J. Phys. Chem.* **1984**, *88*, 1762−1766.
(16) Abdelsalam, M.; Bartlett, P. N.; Russell, A. E.; Baumberg, J. J.; Calvo, E. J.; Tognalli, N. G.; Fainstein, A. Quantitative electrochemical SERS of flavin at a structured silver surface. *Langmuir* **2008**, *24*, 7018−7023.
(17) Xu, H.; Xie, L.; Zhang, H.; Zhang, J. Effect of Graphene Fermi Level on the Raman Scattering Intensity of Molecules on Graphene. *ACS Nano* **2011**, *5*, 5338−5344.
(18) Sriram, S.; Bhaskaran, M.; Chen, S.; Jayawardhana, S.; Stoddart, P. R.; Liu, J. Z.; Medhekar, N. V.; Kalantar-Zadeh, K.; Mitchell, A. Influence of Electric Field on SERS: Frequency Effects, Intensity Changes, and Susceptible Bonds. *J. Am. Chem. Soc.* **2012**, *134*, 4646−4653.
(19) Shi, H.; Poudel, N.; Hou, B.; Shen, L.; Chen, J.; Benderskii, A. V.; Cronin, S. B. Sensing local pH and ion concentration at graphene electrode surfaces using in situ Raman spectroscopy. *Nanoscale* **2018**, *10*, 2398−2403.
(20) Soo Min, K.; Allen, H.; Yi-Hsien, L.; Mildred, D.; Tomás, P.; Ki Kang, K.; Jing, K. The effect of copper pre-cleaning on graphene synthesis. *Nanotechnology* **2013**, *24*, 365602.
(21) Chen, C. C.; Chang, C. C.; Li, Z.; Levi, A. F. J.; Cronin, S. B. Gate tunable graphene-silicon Ohmic/Schottky contacts. *Appl. Phys. Lett.* **2012**, *101*, 223113.
(22) Humbert, C.; Busson, B.; Six, C.; Gayral, A.; Gruselle, M.; Villain, F.; Tadjeddine, A. Sum-frequency generation as a vibrational and electronic probe of the electrochemical interface and thin films. *J. Electroanal. Chem.* **2008**, *621*, 314−321.
(23) Banik, M.; El-Khoury, P. Z.; Nag, A.; Rodriguez-Perez, A.; Guarrottxena, N.; Bazan, G. C.; Apkarian, V. A. Surface-Enhanced Raman Trajectories on a Nano-Dumbbell: Transition from Field to Charge Transfer Plasmons as the Spheres Fuse. *ACS Nano* **2012**, *6*, 10343−10354.
(24) Kwasnieski, D. T.; Wang, H.; Schultz, Z. D. Alkyl-nitrile adlayers as probes of plasmonically induced electric fields. *Chem. Sci.* **2015**, *6*, 4484−4494.
(25) Nelson, D. A.; Schultz, Z. D. Influence of Optically Rectified Electric Fields on the Plasmonic Photocatalysis of 4-Nitrothiophenol and 4-Aminothiophenol to 4,4-Dimercaptoazobenzene. *J. Phys. Chem. C* **2018**, *122*, 8581−8588.
(26) Fried, S. D.; Boxer, S. G. Measuring Electric Fields and Noncovalent Interactions Using the Vibrational Stark Effect. *Acc. Chem. Res.* **2015**, *48*, 998−1006.
(27) Bagchi, S.; Fried, S. D.; Boxer, S. G. A Solvatochromic Model Calibrates Nitriles' Vibrational Frequencies to Electrostatic Fields. *J. Am. Chem. Soc.* **2012**, *134*, 10373−10376.
(28) Schkolnik, G.; Salewski, J.; Millo, D.; Zebger, I.; Franzen, S.; Hildebrandt, P. Vibrational Stark Effect of the Electric-Field Reporter 4-Mercaptobenzonitrile as a Tool for Investigating Electrostatics at Electrode/SAM/Solution Interfaces. *Int. J. Mol. Sci.* **2012**, *13*, 7466−7482.

DOI: 10.1021/acsami.8b11961
ACS Appl. Mater. Interfaces XXXX, XXX, XXX−XXX